Available online at www.sciencedirect.com
ScienceDirect
International Journal of Heat and Mass Transfer 50 (2007) 452–463
International Journal of HEAT and MASS TRANSFER
www.elsevier.com/locate/ijhmt

Assessment of the effectiveness of nanofluids for single-phase and two-phase heat transfer in micro-channels

Jaeseon Lee, Issam Mudawar *

Boiling and Two-Phase Flow Laboratory, School of Mechanical Engineering, Purdue University, West Lafayette, IN 47907, USA

Received 24 March 2006; received in revised form 2 August 2006
Available online 2 October 2006

Abstract

Experiments were performed to explore the micro-channel cooling benefits of water-based nanofluids containing small concentrations of Al_2O_3. The high thermal conductivity of nanoparticles is shown to enhance the single-phase heat transfer coefficient, especially for laminar flow. Higher heat transfer coefficients were achieved mostly in the entrance region of micro-channels. However, the enhancement was weaker in the fully developed region, proving that nanoparticles have an appreciable effect on thermal boundary layer development. Higher concentrations also produced greater sensitivity to heat flux. Despite this enhancement, the overall cooling effectiveness of nanoparticles was quite miniscule because of the large axial temperature rise associated with the decreased specific heat for the nanofluid compared to the base fluid. For two-phase cooling, nanoparticles caused catastrophic failure by depositing into large clusters near the channel exit due to localized evaporation once boiling commenced. These and other practical disadvantages bring into question the overall merit of using nanofluids in micro-channel heat sinks.

1. Introduction

Solid particles generally possess far greater thermal conductivity than common heat transfer liquids. Mixing solid particles in a liquid can therefore enhance the cooling potential of the liquid by increasing the thermal conductivity of the suspended fluid.

In the past, this goal was sought by using relatively large ('milli' or 'micro' scale) particles. While these fluids do provide the aforementioned cooling benefit, their implementation is complicated by their tendency to damage mechanical pumps and valves, as well as clog flow passages due to particle settling.

Recent developments in nanotechnology and related manufacturing techniques have made possible the production of far smaller – nanosized – particles. Such particles greatly reduce the damage to flow loop components while providing the cooling benefits. Choi and co-workers at Argonne National Laboratory proposed the use of nanoparticles to enhance the thermal conductivity of liquids, and coined the term 'nanofluids' for the resulting mixtures [1–3]. Later studies experimentally demonstrated this enhancement effect. Lee et al. [3] used 50 nm or smaller Al_2O_3 and CuO particles to enhance the thermal conductivity of their nanofluids. They showed the percentage enhancement in thermal conductivity was not only a function of concentration and conductivities of the particle material and liquid, but particle size and shape as well. Xuan and Li [4] reported that copper particles provided greater thermal conductivity enhancement than metal oxide particles. Xue [5] showed analytically that carbon nanotubes produce the highest conductivity enhancement of all nanofluids.

The aforementioned clogging problem is perhaps most serious in micro-channel flow devices recently recommended for high-heat-flux electronic and aerospace applications. These devices offer a number of cooling advantages such as high convective heat transfer coefficients, small size and weight, and reduced coolant inventory. Nanofluids are

* Corresponding author. Tel.: +1 765 494 5705; fax: +1 765 494 0539.
E-mail address: mudawar@ecn.purdue.edu (I. Mudawar).

0017-9310/$ - see front matter © 2006 Elsevier Ltd. All rights reserved.
doi:10.1016/j.ijheatmasstransfer.2006.08.001

Nomenclature

CHF	critical heat flux
c_p	specific heat (kJ/kg K)
D	diameter
D_h	hydraulic diameter
f	fanning friction factor
h	heat transfer coefficient (W/m^2 K)
H_{ch}	micro-channel height
H_{tc}	distance from thermocouple to base of micro-channel
k	thermal conductivity (W/m K)
$\dot{m}$	mass flow rate (g/s)
Nu	Nusselt number
n	solid particle shape factor
P	pressure (bar)
Pr	Prandtl number
ΔP	pressure drop (Pa, bar)
Q	heat input to heat sink (W)
q''	heat flux through heat sink base area (W/m^2 or W/cm^2)
Re	Reynolds number based on tube diameter
Re_{Dh}	Reynolds number based on channel hydraulic diameter
T	temperature (°C)
tc	temperature measurement points inside heat sink block
u	mean fluid velocity [m/s]
W_{ch}	micro-channel width
W_w	half-width of copper sidewall
x	axial distance (m)

Greek symbols

η	fin efficiency
μ	viscosity
ρ	density
φ	volumetric concentration of nanoparticles

Subscripts

1,2,3,4	temperature measurement locations
bf	base fluid
ch	channel
D	diameter
HFE 7100	HFE 7100 base fluid
in	channel inlet
m	bulk fluid
nf	nanofluid
out	channel outlet
p	solid particles
s	solid metal for heat sink
sp	single-phase
Water	water base fluid
w	channel wall
x	local condition

considered an ideal fit for micro-channel devices because they are thought to virtually eliminate the clogging problem. Furthermore, they can enhance the already substantial heat transfer coefficients realized with micro-channel flow by the added benefit of greater thermal conductivity.

Investigating the combined advantages of micro-channel flow and nanofluids is precisely the goal of the present study. Those advantages are examined experimentally for both single-phase and two-phase situations, and practical conclusions are drawn concerning the implementation of nanofluids in small coolant passages.

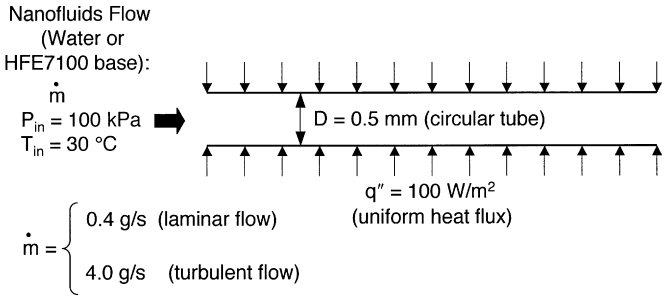

Fig. 1. Uniformly heated flow in circular tube.

2. Enhancement for laminar versus turbulent flow

Aside from thermal conductivity, other fluid properties will change by the particle inclusion, and it is the combined effect of these property variations that dictates the overall enhancement effect for a nanofluid. This point is illustrated with the aid of a simple example that will also show how this effect is quite different for laminar flow as compared to turbulent flow.

Fig. 1 shows a fluid being heated uniformly as it flows inside a circular tube. Ignoring entrance effects for now (these effects will be discussed latter in this paper), the flow is assumed both hydraulically and thermally fully developed. The Nusselt number is constant for laminar flow and follows the Dittus–Boelter equation for turbulent flow.

$$Nu = 4.36 \quad \text{for laminar flow} \tag{1}$$

and

$$Nu = 0.023 Re^{0.8} Pr^{0.4} \quad \text{for turbulent flow} \tag{2}$$

Lee et al. [3] showed that the thermal conductivity of Al_2O_3 nanofluids follows the two-components mixture conductivity model of Hamilton–Crosser model fairly well.

$$k_{nf} = \left[\frac{k_p + (n-1)k_{bf} - (n-1)\varphi(k_{bf} - k_p)}{k_p + (n-1)k_{bf} + \varphi(k_{bf} - k_p)}\right] k_{bf}, \tag{3}$$

where k_{nf}, k_{bf} and k_p are the thermal conductivities of the nanofluid, base fluid and solid particles, respectively, φ is the volumetric concentration of nanoparticles, and n is solid particle shape factor ($n = 3$ for spherical particles).

Following Wen and Ding [6], the Einstein equation is used for dynamic viscosity.

$$\frac{\mu_{nf}}{\mu_{bf}} = 1 + 2.5\varphi, \tag{4}$$

where μ_{nf} and μ_{bf} are the viscosities of the nanofluid and base fluid, respectively.

All other properties are linearized relative to nanoparticle volumetric concentration (Pak and Cho [7]). This yields relationships for density and specific heat, respectively,

$$\rho_{nf} = (1 - \varphi)\rho_{bf} + \varphi\rho_p \tag{5}$$

and

$$c_{p,nf} = (1 - \varphi)c_{p,bf} + \varphi c_{p,p}. \tag{6}$$

The system shown in Fig. 1 yields the following variations of bulk mean fluid temperature and inside wall temperature, respectively, with distance x from the tube entrance.

$$T_{m,x} = T_{in} + \frac{q''\pi Dx}{\dot{m}c_{p,nf}} \tag{7}$$

and

$$T_{w,x} = T_{m,x} + \frac{q''}{h}. \tag{8}$$

Two kinds base fluids are examined in this example, water and HFE-7100. The latter is a 3M dielectric fluid used in electronics cooling and general heat transfer applications. The thermal conductivity for this fluid is significantly smaller than for water. Table 1 shows properties of these base fluids as well as for different concentrations of Al_2O_3.

Fig. 2 shows heat transfer results for the laminar case. For each base fluid, increasing nanoparticle concentration is shown in Fig. 2(a) monotonically increasing the heat transfer coefficient. This is the result of the heat transfer coefficient being proportional to thermal conductivity for laminar flow. Notice that the heat transfer coefficient values with HFE-7100 are much smaller than for water. Overall, the enhancement ratio is almost the same for water and HFE 7100 nanofluids.

However, as shown in Fig. 2(b), increasing nanoparticle concentration increases both fluid and wall temperatures for the nanofluids relative to their base fluid counterparts. This temperature increase is the result of the decreased specific heat of nanofluids caused by the solid particles having lower specific heat than fluids. Notice for HFE-7100 the large axial rise in both fluid and wall temperature. This trend is the result of the small specific heat for this fluid.

Fig. 3 shows the results for the turbulent case. According to Eq. (2), $h \sim k^{0.6}$ for turbulent flow compared to $h \sim k$ for laminar flow. This implies the enhancement effect

Table 1
Al_2O_3 nanoparticle suspension fluid properties at 30 °C and 100 kPa

	Water base						HFE 7100 base					
	$\varphi = 0\%$	1%	2%	3%	4%	5%	$\varphi = 0\%$	1%	2%	3%	4%	5%
k_{nf} (W/m K)	0.603	0.620	0.638	0.656	0.675	0.693	0.0678	0.0699	0.0720	0.0741	0.0763	0.0785
ρ_{nf} (kg/m^3)	995.7	1021.7	1047.7	1073.8	1099.8	1125.9	1455.4	1476.9	1498.3	1519.8	1541.2	1562.7
μ_{nf} (kg/m s)	7.977×10^{-4}	8.177×10^{-4}	8.376×10^{-4}	8.576×10^{-4}	8.775×10^{-4}	8.974×10^{-4}	6.556×10^{-4}	6.720×10^{-4}	6.884×10^{-4}	7.048×10^{-4}	7.212×10^{-4}	7.376×10^{-4}
$c_{p,nf}$ (kJ/kg K)	4.183	4.149	4.115	4.081	4.046	4.012	1.193	1.189	1.184	1.180	1.176	1.172

Solid (Al_2O_3) properties: $\rho_s = 3600$ kg/m^3, $k_s = 36.0$ W/m K, $c_{p,s} = 0.765$ kJ/kg K.

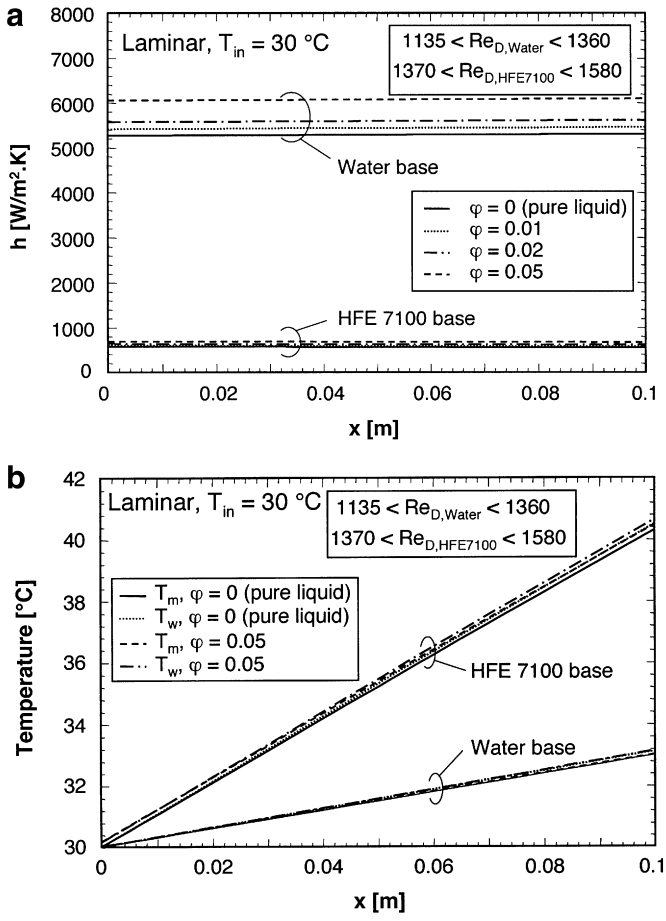

Fig. 2. Axial variations of (a) heat transfer coefficient and (b) bulk and wall temperatures for laminar flow and different nanoparticle concentrations in water and HFE7100 base fluids.

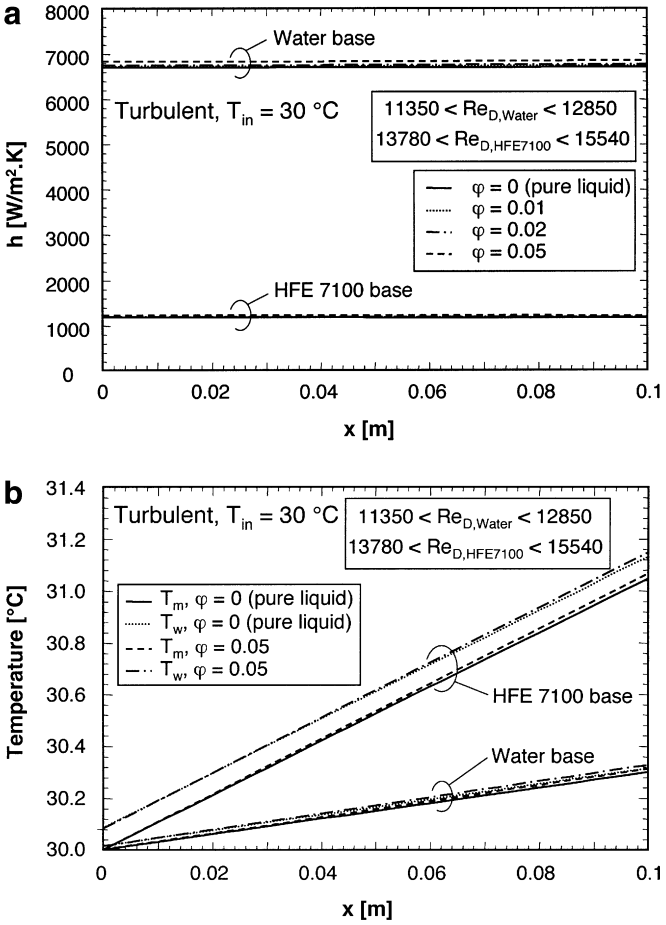

Fig. 3. Axial variations of (a) heat transfer coefficient and (b) bulk and wall temperatures for turbulent flow and different nanoparticle concentrations in water and HFE7100 base fluids.

due to the increased thermal conductivity of nanofluids is significantly weaker for turbulent flow than for laminar. The enhancement in turbulent flow is also dependent on flow rate in addition to viscosity and specific heat. Since $h \sim k^{0.6}\mu^{-0.4}c_p^{0.4}$, and because increased nanoparticle concentration enhances viscosity and degrades specific heat, the enhancement effect of nanoparticles in turbulent flow is further reduced compared to thermal conductivity alone. This effect is quite evident in Fig. 3(a).

This simple analysis shows how the enhancement effect of nanofluids is more effectively realized in laminar flow. Interestingly, most micro-channel flows of practical interest are laminar because of both their small hydraulic diameter and small flow rates. Implementing nanofluids in micro-channel devices therefore appears to be an advantageous strategy in pursuit of enhanced cooling performance.

3. Experimental methods

3.1. Nanofluid preparation

The solid particles used in this study were Al_2O_3. The nanofluid was produced by gas condensation by Nanophase Technologies. Insoluble solid Al_2O_3 particles with an area-averaged size of about 36 nm came dispersed in high concentration in water, which formed the base fluid. This high concentration fluid was diluted with de-ionized water to the desired specified volume concentration demanded for individual experiments.

Two volumetric concentrations of Al_2O_3 nanofluid, 1% and 2%, were tested in the present study. The particle size and shape were identical to those used by Lee et al. [3], who measured about 6% enhancement in thermal conductivity with 2% Al_2O_3.

3.2. Test loop and operating procedure

The enhancement effects of the Al_2O_3 nanofluids were examined with the aid of a test facility that was used in earlier studies of single-phase and two-phase micro-channel heat sink performance by Qu and Mudawar [8–10]. As shown in Fig. 4, water was pumped from a reservoir through a filter followed by one of two parallel flowmeters, and a constant-temperature bath before entering the micro-channel test module. Exiting the test module, the fluid was passed through a water-cooled condenser before returning

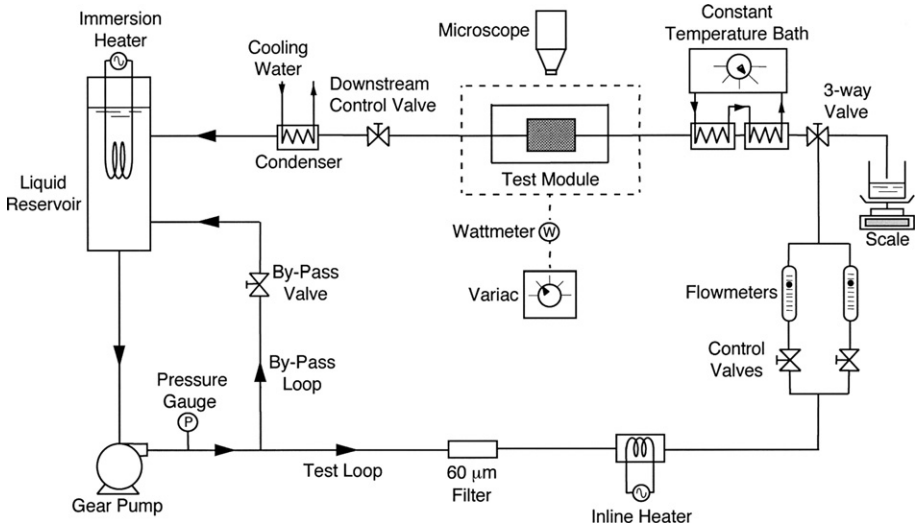

Fig. 4. Schematic of flow loop.

to the reservoir. Since the flow meters were not calibrated for the 1% and 2% Al_2O_3 concentrations, a bypass was included immediately downstream of the flowmeters to calibrate the flowmeters for these concentrations. The calibration was achieved by dividing the mass of nanofluid accumulated in a beaker by the fill time. A precision digital bench scale was used for the mass measurements.

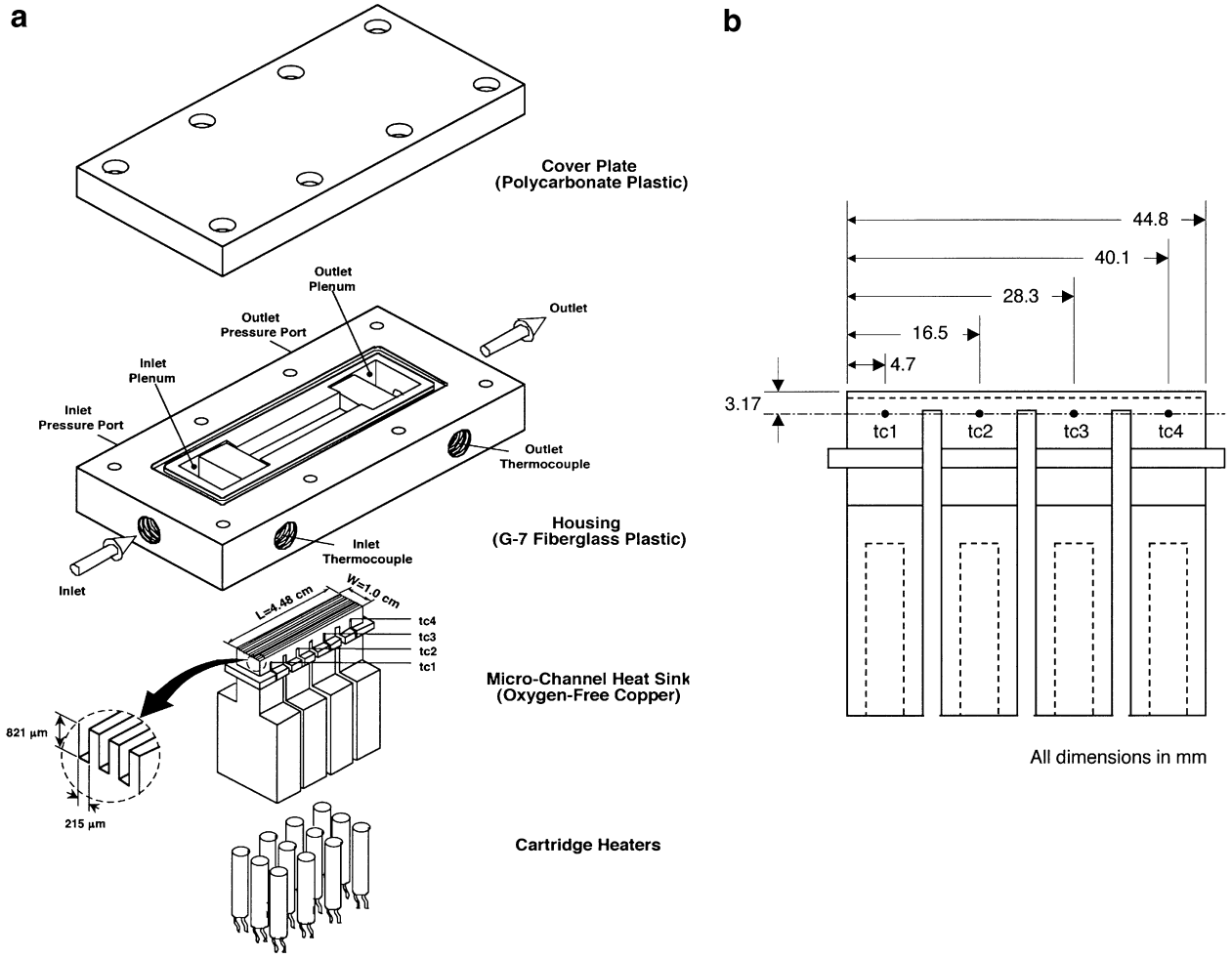

Fig. 5. (a) Construction of micro-channel test module and (b) thermocouple locations in copper block inside test module.

Fig. 5 shows a schematic of the micro-channel test module. Rectangular 215 μm wide by 821 μm deep grooves were milled into the top surface of an oxygen-free copper block. This block was inserted into a G-7 plastic housing and sealed atop with a polycarbonate plastic cover plate. This formed 21 parallel micro-channels with a hydraulic diameter of 341 μm and a total planform area 1 cm wide by 4.48 cm long. Heating was provided by 12 cartridge heaters that were embedded in the underside of the copper block. The G-7 housing featured inlet and exit plenums where the fluid temperature and pressure were measured with the aid of type-K thermocouples and pressure transducers, respectively.

Fig. 5(b) shows the detailed construction of the copper block. Notice the three deep cuts in the copper block virtually dividing the block into four cells, which helped confine the power dissipated by each set of cartridge heaters to the micro-channel flow region immediately above, thus minimizing axial heat flow. Four type-K thermocouples were inserted along the flow direction to determine the channel bottom wall temperatures. A Yokogawa WT210 power meter measured electric power input to the copper block. All the facility's sensor signals were input to an HP 3852A data acquisition system.

Cooling performances of the nanofluids were benchmarked against that for pure water. The pure water experiments were performed first. The test facility was drained completely and flushed very carefully with de-ionized water before it was filled with a new fluid. Operating conditions for the study were as follows: $Re_{Dh} = 140$–941, $Q = 100$–300 W, $T_{in} = 30$ °C, $P_{in} = 1.17$–1.36 bar, and $P_{out} = 1.12$ bar.

Measurement uncertainties were ±0.3 °C for temperature, 0.5% for pressure, 0.1% for electrical power, and 2% for flow rate. Heat loss from the copper block was estimated at less than 5% of the electrical power input.

4. Single-phase results

4.1. Pressure drop

Suspending solid particles in a fluid generally increases dynamic viscosity relative to the base fluid. Even with nanoparticles, this phenomenon causes a pressure drop increase in micro-channels compared to an equal mass flow rate of the base fluid.

Since the present pressure measurements were made in the inlet and outlet plenums of the test module, they included inlet contraction pressure loss and outlet expansion pressure recovery in addition to the pressure drop along the micro-channels as detailed by Qu and Mudawar for pure water [8].

Fig. 6(a) shows the variation of the measured pressure drop between the inlet and outlet plenums with Reynolds number for adiabatic flow. A strong particle concentration dependency is shown with the total pressure drop increasing with increasing nanoparticle concentration. Instead of using the viscosity relation given earlier in Eq. (4), Re_{Dh} in Fig. 6(b) was based an empirical relation developed specifically for water-based Al_2O_3 nanofluids [11],

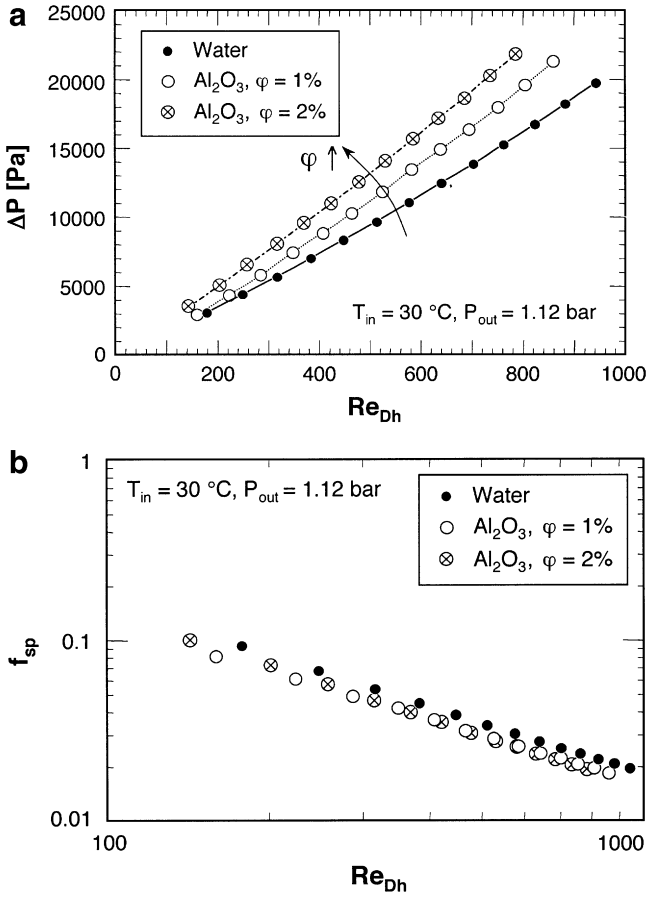

Fig. 6. Variations of (a) pressure drop across test module and (b) friction factor across micro-channels with Reynolds number for pure water and for 1% and 2% Al_2O_3.

$$\frac{\mu_{nf}}{\mu_{bf}} = 123\varphi^2 + 7.3\varphi + 1. \tag{9}$$

After subtracting the effects of inlet contraction and outlet expansion from the total measured pressure drop (see Ref. [8] for detailed calculation scheme), a single-phase micro-channel friction factor was determined from the pressure drop ΔP_{ch} calculated for the micro-channels alone.

$$f_{sp} = \frac{\Delta P_{ch} D_h}{2L\rho_f u^2}. \tag{10}$$

Fig. 6(b) shows particle concentration does not have a clear influence on the friction factor dependence on Reynolds number. Error propagation from measurement uncertainties is estimated at 2.9% in the friction factor calculation.

4.2. Heat transfer coefficient

The single-phase heat transfer coefficient was determined from the measured fluid and heater block temperatures and

the electrical power input using an analytical fin technique detailed by Qu and Mudawar [9].

Fig. 7 shows a unit control volume consisting of a single micro-channel and half of the surrounding copper walls. Equating the heat influx to the unit cell through the bottom solid wall to the heat efflux yields

$$q''(W_{ch} + 2W_w) = h_{sp}(T_w - T_m)(W_{ch} + 2\eta H_{ch}), \tag{11}$$

where η is the fin efficiency. Since the top wall is adiabatic, the fin efficiency is given by

$$\eta = \frac{\tanh mH_{ch}}{mH_{ch}}, \tag{12}$$

where m is the fin parameter defined as

$$m = \sqrt{\frac{h_{sp}}{k_s W_w}}. \tag{13}$$

These three equations were used to determine the single-phase heat transfer coefficient, h_{sp}. The corresponding error propagation from measurement uncertainties is estimated at 5.0%.

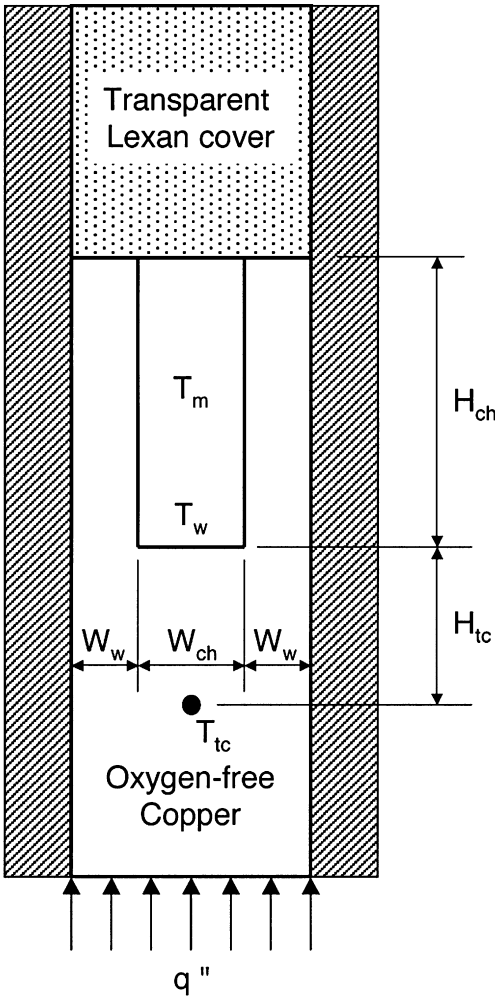

Fig. 7. Micro-channel unit cell.

The fin base temperature, T_w, was calculated using the assumption of one-dimensional heat diffusion between the plane of the thermocouple embedded in the copper block and the plane containing the fin base.

$$T_w = T_{tc} - \frac{q''H_{tc}}{k_s}. \tag{14}$$

Fig. 8 shows the variation of the single-phase heat transfer coefficient along the flow direction for water and the two nanofluids for different power inputs. The four measurement locations correspond to the thermocouple layout shown earlier in Fig. 5(b). The two upstream locations are well within the entrance region, while the third and the fourth indicate the flow is becoming thermally fully developed. The nanofluids exhibit the same spatial trend as that for pure water. Fig. 8(a) and (b) show similar trends for 1% and 2% Al_2O_3, respectively, as compared to pure water. In each of these figures, increasing the heat flux has a very weak effect on the heat transfer coefficient for pure water, but an appreciable effect for the nanofluid. Notice also the stronger effect of heat flux for 2% Al_2O_3, Fig. 8(b), compared to 1% Al_2O_3, Fig. 8(a).

Keblinski et al. [12] suggested four possible mechanisms for heat transfer enhancement with nanofluids: Brownian

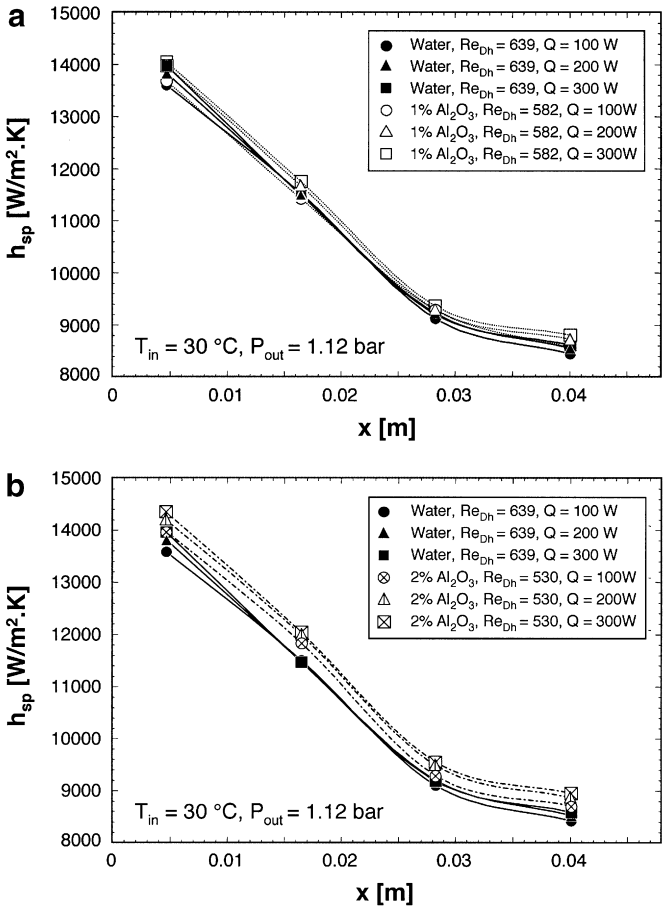

Fig. 8. Variation of heat transfer coefficient along micro-channel for (a) pure water and 1% Al_2O_3, and (b) pure water and 2% Al_2O_3.

motion, liquid layering at liquid/particle interface, phonon movement in nanoparticles, and nanoparticle clustering. While it is difficult to determine which of these four mechanisms has the greatest impact on enhancement, the increased dependence of the heat transfer enhancement on heat flux at higher concentrations may be one trend future research may rely upon in pursuit of mechanism identification. In any case, this increased dependence appears to alter boundary layer development for nanofluids.

Fig. 9 compares the heat transfer coefficient variation with Reynolds number for water, 1% Al_2O_3 and 2% Al_2O_3 for each of the four axial locations along the micro-channel heat sink. For each axial location, 2% Al_2O_3 shows the greatest heat transfer enhancement. For 1% Al_2O_3, the enhancement is obvious for the first two upstream locations, but virtually nonexistent for the two downstream locations where the thermal boundary layer is almost fully developed. In fact, the enhancement effect for both concentrations appears far more prevalent in the entrance region than the downstream fully developed region. It can therefore be concluded that nanoparticles have an appreciable effect on thermal boundary layer development.

Interestingly, this trend is a general agreement with the findings of Wen and Ding [6] for Al_2O_3 nanofluid flow inside a much larger tube ($D = 4.5$ mm).

4.3. Axial variations of fluid and wall temperatures

As discussed earlier, the thermal performance of a heat sink is dictated not only by the magnitude of the heat transfer coefficient, but by the wall temperature of the heat sink as well. Increasing nanoparticle concentration increases the fluid's thermal conductivity, thus increasing the heat transfer coefficient, especially for laminar flow. On the other hand, increased nanoparticle concentration also degrades specific heat, resulting in larger axial rises in both fluid and wall temperatures compared to the base fluid. Therefore, it is not immediately evident if the wall temperature actually decreases (a sign of better cooling performance) with increasing nanoparticle concentration as a result of the higher heat transfer coefficient, given this degradation in the nanofluid's specific heat.

Fig. 10 shows the measured variation of mean fluid temperature between the inlet and outlet of the micro-channel heat sink with mass flow rate. Shown is an increase in temperature difference with increased nanoparticle concentration due to the specific heat degradation. This effect is more pronounced for lower mass flow rates and higher heat fluxes.

Fig. 11 shows the net effect of increasing thermal conductivity and decreasing specific heat on the wall temperature, which is perhaps the most realistic measure of the effectiveness of a given cooling scheme. These wall

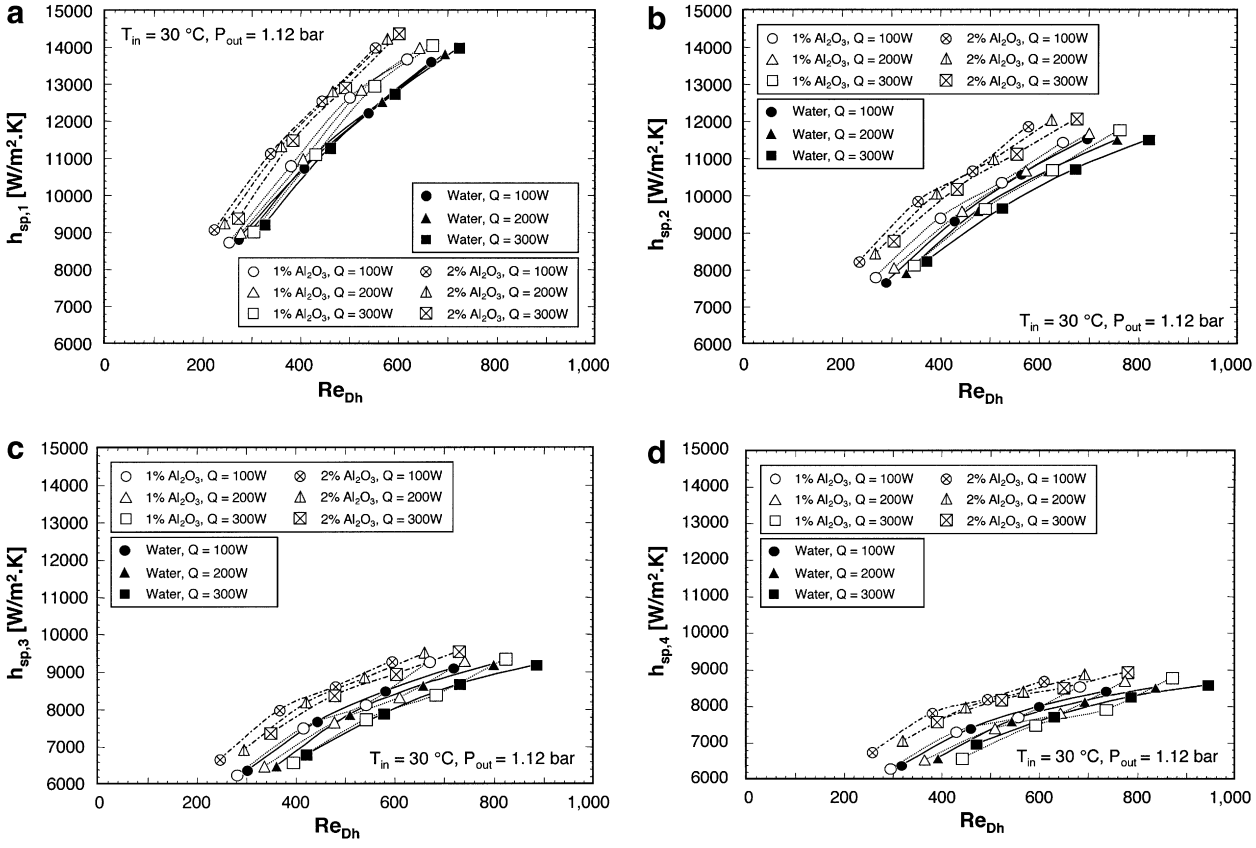

Fig. 9. Variation of heat transfer coefficient with Reynolds number for different heat inputs and different Al_2O_3 concentrations at measurement locations (a) tc1, (b) tc2, (c) tc3, and (d) tc4.

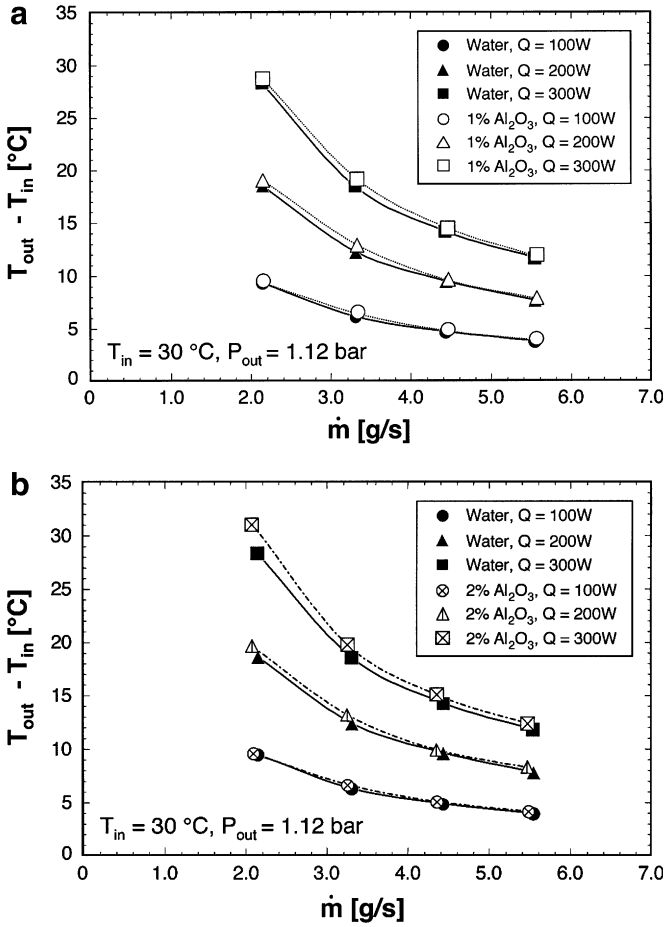

Fig. 10. Variation of fluid temperature rise along micro-channel for (a) pure water flow and 1% Al_2O_3, and (b) pure water and 2% Al_2O_3.

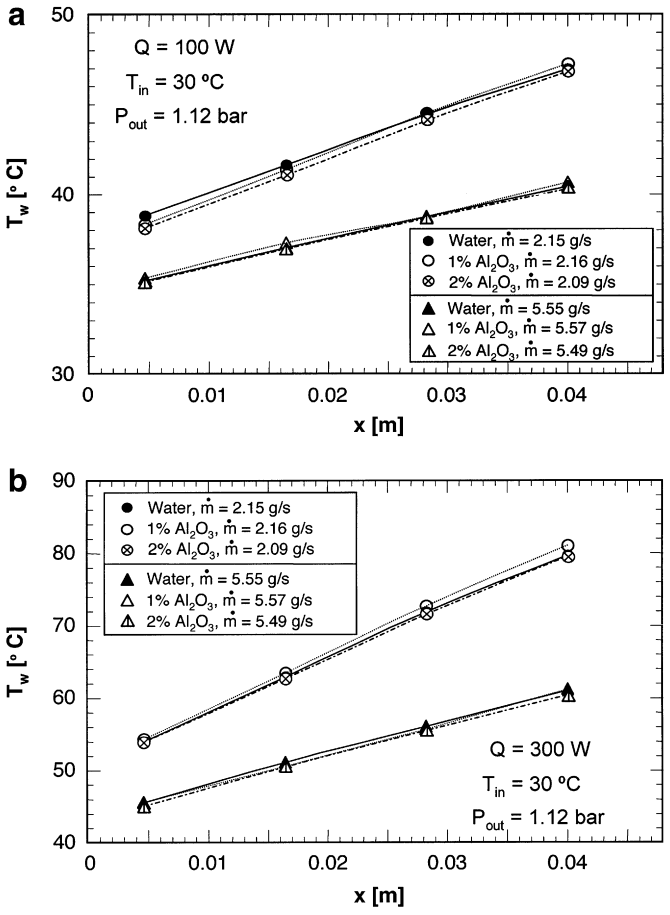

Fig. 11. Variation of wall temperature along micro-channel for different flow rates and Al_2O_3 concentrations and heat inputs of (a) 100 W and (b) 300 W.

temperatures were calculated using Eq. (14) with measured thermocouple data. The only noticeable decrease in wall temperature is realized near the inlet for the lower mass flow rate at the lower heat input. All other conditions and axial locations show virtually no measurable enhancement. Furthermore, any differences in the wall temperature are within the range of measurement uncertainty of the study, let alone the difficulty of achieving an exact flow rate when comparing different cases. These findings prove nanoparticles are not an effective means for enhancing single-phase cooling performance of a micro-channel heat sink.

4.4. Fluid stability

Particle settlement is an obvious concern with solid particle suspensions that are intended for cooling applications. As mentioned earlier, nanoparticle suspensions are far more stable than suspensions of larger particles.

This issue was examined in the present study by repeating heat transfer coefficient measurements in tests that were separated by many hours. Fig. 12(a) and (b) shows these results for 2% Al_2O_3 and Reynolds numbers of 202 and 530, respectively. These results show fairly repeatable results over the indicated time span.

Another method of assessing nanofluid stability was to visually inspect fluid samples over an extended period of time. The samples were sealed in glass beaker for the entire period. Fig. 13 compares picture of 1% and 2% Al_2O_3 nanofluids taken shortly after initial mixing and 30 days later. The latter pictures show some settlement and a concentration gradient in both nanofluids. Such effects can cause long-term degradation in thermal performance due to settling inside the cooling system's reservoir. Furthermore, most cooling systems contain feedback control systems that attenuate coolant flow rate or stop it altogether in response to the fluctuating heat load of the device being cooled. Slow or zero flow rate accentuate nanoparticle settling and may even lead to clogging of individual components of the cooling loop. This issue points to the need for long-term testing of a nanofluid cooling loop before actual deployment.

Another long-term concern with nanofluids is surface abrasion. Like most metal surfaces, copper exhibits some oxidation when exposed to pure water. This effect was more pronounced with increasing surface temperature.

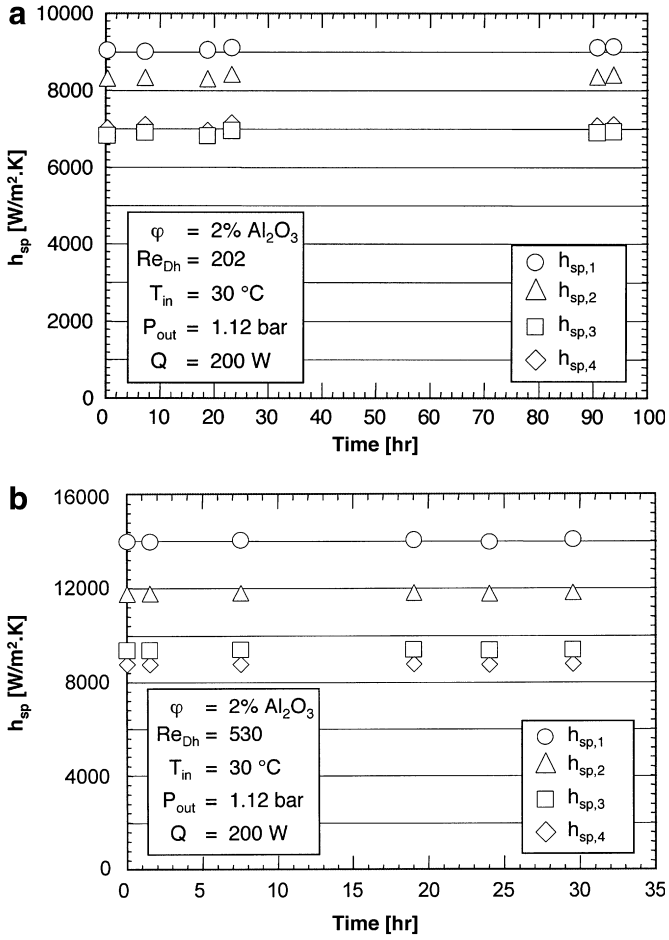

Fig. 12. Heat transfer coefficient versus time for 2% Al_2O_3 and Reynolds numbers of (a) 202 and (b) 530.

The oxidize layer acts as an additional thermal resistance and tends to degrade the heat transfer performance. Interestingly, the micro-channel surface appeared cleaner and shinier following each single-phase experiment with the nanofluids. This phenomenon is believed to be the result of erosion of the copper surface by the nanoparticles. While this may seem an advantage for nanofluids, special attention must be paid to the possibility of the removed oxide getting entrained with the flow, altering the enhancement effect of the nanoparticles, and contributing long term to particle settling or even clogging of flow passages.

5. Flow boiling results

Flow boiling can greatly enhance the cooling performance of a micro-channel heat sink by increasing the heat transfer coefficient. Furthermore, since flow boiling relies to a great degree on latent heat transfer, better temperature axial uniformity is realized both in the coolant and the wall compared to a single-phase heat sink. The question here is whether nanoparticles could further enhance an already superior performance.

Recently, several research articles examined the effects of nanoparticles on pool boiling [13–15]. Degradation in nucleate boiling performance was related to surface smoothing, resulting from bubble-generated cavity filling with particles and particle deposition on the heating surface. However, nanofluids netted a measurable increase in critical heat flux (CHF).

In this research, flow boiling experiments were conducted with the micro-channel heat sink using pure water and 1% Al_2O_3. Fig. 14(a) shows the data for pure water follow a typical boiling curve. This curve is initiated at low heat fluxes with single-phase forced convection, followed by an appreciable slope change following the onset of boiling, and culminating in a sudden unsteady temperature rise at CHF. While single-phase forced convection proceeded in the same manner with increasing heat flux for 1% Al_2O_3, flow boiling was never achieved with this nanofluid. It appears fluid evaporation associated with the initial incipience of boiling near the channel exit caused rapid deposition of nanoparticles in the same region. Despite the small size of these particles, the deposition rate was so severe that relatively large particle clusters could be seen near the exit. This clustering effect quickly propagated upstream and filled the entire channel, preventing the coolant from entering the heat sink. The heat sink responded with a sudden

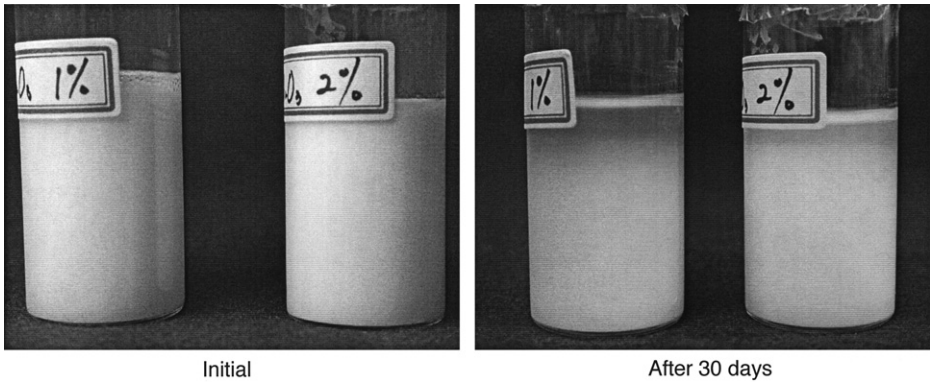

Fig. 13. Nanofluid settling over 30-day period.

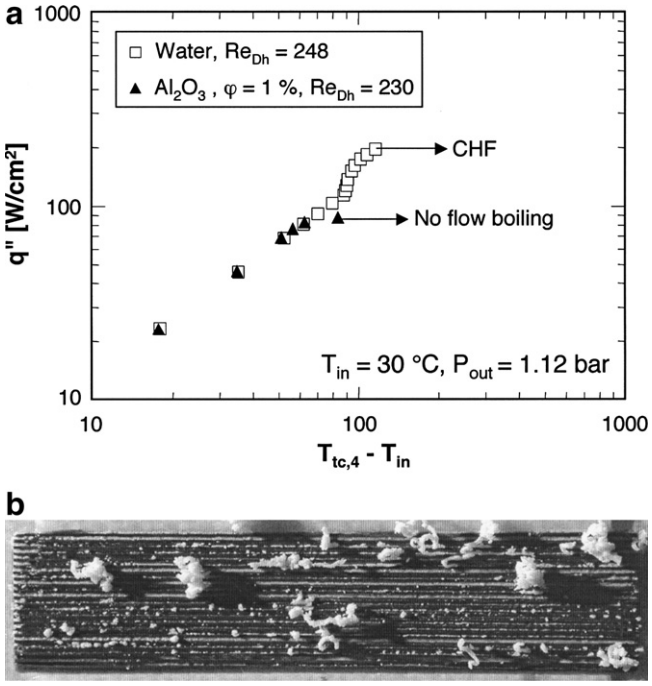

Fig. 14. (a) Flow boiling curve at measurement location tc4 for pure water and 1% Al_2O_3 and (b) photo of particles after being removed from micro-channels.

unsteady temperature rise. This phenomenon constitutes a catastrophic failure for a cooling system. Fig. 14(b) shows photos of the deposited particles after they were removed by a fine needle.

6. Conclusions

This study is an assessment of the effectiveness of Al_2O_3 nanoparticles at enhancing single-phase and two-phase heat transfer in micro-channel heat sinks. Key conclusions can be summarized as follows:

(1) The high thermal conductivity of nanoparticles relative to common pure fluids enhances the single-phase heat transfer coefficient for fully-developed laminar flow. The enhancement is far weaker for turbulent flow because of a weaker dependence of the heat transfer coefficient on thermal conductivity as well as decreased specific heat and increased viscosity with increased nanoparticle concentration.
(2) Increasing nanoparticle concentration increases single-phase pressure drop compared to pure fluids at the same Reynolds number.
(3) Higher single-phase heat transfer coefficients are achieved in the entrance region of micro-channels with increased nanoparticle concentration. However, the enhancement is weaker in the fully developed region, proving that nanoparticles have an appreciable effect on thermal boundary layer development. Higher concentrations also produce greater sensitivity to heat flux.
(4) Despite their ability to enhance to the single-phase heat transfer coefficient due to the increased thermal conductivity, the overall cooling effectiveness of nanopartcles is quite miniscule. Simultaneous degradation of the specific heat leads to larger fluid temperature rise along the micro-channel. The net effect of increasing thermal conductivity and decreasing specific heat on wall temperature is virtually non-existent.
(5) Single-phase cooling performance with nanofluids is quite repeatable over extended durations. However, very long-term use may lead to particle settling and potential clogging of flow passages. This issue must me carefully examined by long term testing of the entire cooling system, including variations of, or complete stoppage of the coolant flow rate, before deployment. Nanoparticles also cause erosion to metal surfaces and, while this may help maintain surface texture, the removed oxide may ultimately alter the enhancement effect of nanoparticles, accentuate settling, or even clog flow passages.
(6) Nanoparticles should not be used in two-phase micro-channel heat sinks. Once boiling commences, particles begin to deposit into relatively large clusters near the channel exit due to localized evaporation. This clustering phenomenon quickly propagates upstream to fill the entire channel, preventing coolant from entering the heat sink and causing catastrophic failure of the cooling system.

Table 2 summarizes the practical implications from the present study. While this study does demonstrate the effectiveness of nanoparticles at enhancing the single-phase heat transfer coefficient by increasing the nanofluids thermal conductivity, it also shows only a miniscule enhancement in cooling effectiveness compared to the pure fluid, and reveals several important disadvantages. These disadvantages bring into question the overall merit of using nanofluids in micro-channel heat sinks. A far more effective strategy may be to simply optimize micro-channel geo-

Table 2
Advantages and disadvantages of nanofluids

Advantages	Disadvantages
Higher single-phase heat transfer coefficient, especially for laminar flow, due to increased thermal conductivity	Increased axial rise in wall temperature due to degraded specific heat
	Increase pumping power due to greater pressure drop
	Long-term fluid settling and potential clogging of flow passages
	Possible damage to flow loop parts by erosion
	Inability to sustain flow boiling
	High cost of nanoparticle suspensions

metry in pursuit of a higher heat transfer coefficient and lower pressure drop using pure fluids [16,17].

Acknowledgements

The authors greatly appreciate the support of the Office of Naval Research (ONR) for this study.

References

[1] S.U.S. Choi, Enhancing thermal conductivity of fluids with nanoparticles. Developments and Applications of Non-Newtonian Flows, FED-vol. 231/MD-vol. 66, ASME, New York, 1995, pp. 99–105.
[2] S. Lee, S.U.S. Choi, Application of metallic nanoparticle suspension in advanced cooling systems. Recent Advances in Solids/Structures and Applications of Metallic Materials, PVP-vol. 342/MD-vol. 72, ASME, New York, 1996, pp. 227–234.
[3] S. Lee, S.U.-S. Choi, S. Li, J.A. Eastman, Measuring thermal conductivity of fluids containing oxide nanoparticles, ASME J. Heat Transfer 121 (1999) 280–289.
[4] Y. Xuan, Q. Li, Heat transfer enhancement of nanofluids, Int. J. Heat Fluid Flow 21 (2000) 58–64.
[5] Q.-Z. Xue, Model for effective thermal conductivity of nanofluids, Phys. Lett. A 307 (2003) 313–317.
[6] D. Wen, Y. Ding, Experimental investigation into convective heat transfer of nanofluids at the entrance region under laminar flow conditions, Int. J. Heat Mass Transfer 47 (2004) 5181–5188.
[7] B.C. Pak, Y.I. Cho, Hydrodynamic and heat transfer study of dispersed fluids with submicron metallic oxide particles, Exp. Heat transfer 11 (1998) 151–170.
[8] W. Qu, I. Mudawar, Experimental and numerical study of pressure drop and heat transfer in a single-phase micro-channel heat sink, Int. J. Heat Mass Transfer 45 (2002) 2549–2565.
[9] W. Qu, I. Mudawar, Flow boiling heat transfer in two-phase micro-channel heat sinks – I. Experimental investigation and assessment of correlation methods, Int. J. Heat Mass Transfer 46 (2003) 2755–2771.
[10] W. Qu, I. Mudawar, Measurement and correlation of critical heat flux in two-phase micro-channel heat sinks, Int. J. Heat Mass Transfer 47 (2004) 2045–2059.
[11] S.E.B. Maiga, C.T. Nguyen, N. Galanis, G. Roy, Heat transfer behaviours of nanofluids in an uniformly heated tube, Superlattices Microstruct. 35 (2004) 543–557.
[12] P. Keblinkski, S.R. Phillpot, S.U.S. Choi, J.A. Eastman, Mechanisms of heat flow in suspensions of nano-sized particles (nanofluids), Int. J. Heat Mass Transfer 45 (2002) 855–863.
[13] S.K. Das, N. Putra, W. Roetzel, Pool boiling of nano-fluids on horizontal narrow tubes, Int. J. Multiphase Flow 29 (2003) 1237–1247.
[14] I.C. Bang, S.H. Chang, Boiling heat transfer performance and phenomena of Al_2O_3-water nano-fluids from a plain surface in a pool, Int. J. Heat Mass Transfer 48 (2005) 2407–2419.
[15] P. Vassallo, R. Kumar, S. D'Amico, Pool boiling heat transfer experiments in silica–water nano-fluids, Int. J. Heat Mass Transfer 47 (2004) 407–411.
[16] W. Qu, I. Mudawar, A systematic method for optimal design of two-phase micro-channel heat sinks, ASME J. Electron. Packaging 127 (2005) 381–390.
[17] J. Lee, I. Mudawar, Implementation of micro-channel evaporator for high-heat-flux refrigeration cooling applications, ASME J. Electron. Packaging 128 (2006) 30–37.